J. Fluid Mech. (1997), *vol.* 340, *pp.* 225–247. Printed in the United Kingdom

Interaction of isotropic turbulence with shock waves: effect of shock strength

By SANGSAN LEE†, SANJIVA K. LELE AND PARVIZ MOIN

Center for Turbulence Research, Stanford University, Stanford, CA 94305-3030, USA

(Received 11 November 1994 and in revised form 8 October 1996)

As an extension of the authors' work on isotropic vortical turbulence interacting with a shock wave (Lee, Lele & Moin 1993), direct numerical simulation and linear analysis are performed for stronger shock waves to investigate the effects of the upstream shock-normal Mach number (M_1). A shock-capturing scheme is developed to accurately simulate the unsteady interaction of turbulence with shock waves. Turbulence kinetic energy is amplified across the shock wave, and this amplification tends to saturate beyond $M_1 = 3.0$. An existing controversy between experiments and theoretical predictions on length scale change is thoroughly investigated through the shock-capturing simulation: most turbulence length scales decrease across the shock, while the dissipation length scale ($\overline{\rho}q^3/\epsilon$) increases slightly for shock waves with $M_1 < 1.65$. Fluctuations in thermodynamic variables behind the shock wave are nearly isentropic for $M_1 < 1.2$, and deviate significantly from isentropy for the stronger shock waves, due to the entropy fluctuation generated through the interaction.

1. Introduction

The interaction between shock waves and turbulent boundary layers is common in high-speed flows. A fundamental understanding of the interaction is important to develop engineering models. There has been a significant accumulation of experimental data on shock/turbulence interaction during the last decade. The interaction of turbulent boundary layers with a shock wave over a compression corner was investigated by Dolling & Or (1985), Andreopoulos & Muck (1987), and Smits & Muck (1987). A general finding from these experiments is that Reynolds shear stress and turbulence intensities are amplified across the shock wave. The studies of oblique shock wave/turbulent boundary layer interaction include several additional complex phenomena, such as wall proximity, unsteady shock stem movement, boundary layer separation, and boundary layer curvature along the compression corner (Honkan & Andreopoulos 1992). To isolate the effects of a shock wave on turbulence, several experiments (Debieve & Lacharme 1986; Keller & Merzkirch 1990; Honkan & Andreopoulos 1992) on the interaction between the shock wave and grid-generated turbulence have been performed. An important finding is that turbulence is amplified and turbulence length scales *increase* across the shock wave. However, the increase in the length scale contradicts the intuitive expectation that mean flow compression should decrease the relevant turbulence length scales. This issue of length scale change across the shock will be discussed extensively in the present paper. Recently,

† Present address: SERI/KIST, PO Box 1, Yuseong, Daejeon 305-600, Republic of Korea.

Barre, Alem & Bonnet (1996) have experimentally studied the interaction of quasi-homogeneous turbulence with a normal shock wave at $M_1 = 3$. Amplification of turbulence in accord with Ribner's theory, and a substantial decrease of the longitudinal integral scale across the shock is reported. These findings are in qualitative agreement with results of the present paper.

Small-amplitude fluctuations in compressible turbulence can be decomposed into three modes of mutually independent fluctuations: vortical, acoustic, and entropic (Kovásznay 1953). Any one of the elementary waves interacting with a shock wave generates all three modes of fluctuations downstream of the shock wave. Since the 1950s, linear interaction analyses (LIA) on the modification of elementary disturbance waves by the shock wave have been performed with an emphasis on the acoustic wave generation behind the shock wave (Ribner 1953, 1954, 1987; Moore 1953; Kerrebrock 1956; Chang 1957; McKenzie & Westphal 1968). Through the linear analyses, turbulent fluctuations downstream of the shock wave are expressed in terms of the orientation, amplitude, and length scale of an incident elementary wave. Inspection of the linear analysis reveals three major factors in the interaction: mean flow compression across the shock, shock front curvature, and unsteady shock front movement. In general, fluctuations are found to be amplified with length scales decreased across the shock wave. Significant acoustic noise is also found to be generated due to the interaction of vortical turbulence with the shock wave. The linear analysis was revisited by Anyiwo & Bushnell (1982) to identify primary mechanisms of turbulence enhancement: amplification of the vorticity mode, generation of acoustic and entropy modes from the interaction, and turbulence 'pumping' by shock oscillations. Zang, Hussaini & Bushnell (1984) performed numerical computations of elementary waves interacting with a shock wave to investigate the effects of shock strength, incidence angle and amplitude of incoming waves on the applicability of the linear analyses. It was found that the linear analyses were valid for wide range of these parameters. For waves incident near the critical angle significant nonlinear effects were also noted. Recently, the applicability of homogeneous rapid distortion theory (RDT) on shock/turbulence interaction was investigated by Jacquin, Cambon & Blin (1993). RDT was found inappropriate for the analysis of shock/turbulence interaction, since the shock front curvature and the shock front unsteadiness cannot be accounted for in the analysis.

Numerical simulations of the shock/turbulence interaction are just beginning to emerge. Using a shock-capturing numerical technique on the Euler equations, Rotman (1991) calculated the change in a two-dimensional turbulent flow caused by the passage of a travelling shock wave. He found that the shock causes an increase in the turbulent kinetic energy and that turbulence length scales are reduced upon passage of the shock. Lee, Lele & Moin (1991*a*) and Lee, Moin & Lele (1992*b*) conducted direct numerical simulations of two- and three-dimensional turbulence interacting with a shock wave. They found that the vorticity amplification compared well with the linear analysis predictions, and turbulent kinetic energy undergoes a rapid increase behind the shock wave. The spectrum was found to be enhanced more at large wavenumbers, leading to an overall length scale decrease. The unsteady corrugation of the shock front was examined. The characteristic speed and slope of the corrugated shock front were found to scale with the upstream r.m.s. velocity fluctuation and the upstream turbulence intensity, respectively.

This paper is an extension of the work of Lee, Lele & Moin (1993) on isotropic turbulence interacting with a weak shock wave, where the upstream mean flow Mach number, M_1, was less than 1.2. In the present paper the interaction of isotropic

turbulence with stronger shock waves is studied. Our objective is to investigate the effects of shock strength on turbulence modification. Numerical simulation and linear analysis are used for this purpose. This paper is organized as follows. §2 discusses the development and validation of the numerical scheme. Ribner's (1954) linear analysis is also briefly summarized. Results from the simulations and analysis are then presented in section 3. The influence of shock Mach number on the turbulent kinetic energy, turbulence length scale, and thermodynamic fluctuations is discussed. The exisiting controversy on the influence of the shock on the turbulence length scale is emphasized.

2. Numerical simulation and linear theory

2.1. *Shock-capturing scheme*

For the direct numerical simulation (DNS) of the interaction of isotropic turbulence with a weak shock wave, the shock wave structure was resolved as a solution of the Navier–Stokes equations. In addition, all the essential turbulence scales were resolved (Lee *et al.* 1993). However, for stronger shock waves resolving the shock structure is unnecessary since the Navier–Stokes equations are no longer valid inside the shock wave (see e.g. Sherman 1955). Furthermore the thickness of the shock decreases as its Mach number increases, making it extremely difficult to cope numerically with very thin shocks. Traditional central difference schemes generate spurious oscillations if sharp gradients in the solution are not resolved. Therefore, a shock-capturing scheme is necessary. The shock-capturing scheme is required to be high-order accurate throughout the computational domain (to properly simulate the evolution of turbulence) as well as to be able to give a smooth and accurate transition across the shock wave. The shock-capturing scheme used in this work is an essentially non-oscillatory (ENO) scheme (Harten & Osher 1987; Shu & Osher 1989), which can be constructed to a high order of accuracy. The ENO scheme used in this paper is based on the Lax–Friedrichs scheme with an interpolation on fluxes. For two- and three-dimensional cases the ENO scheme is applied independently for fluxes in each direction (Shu & Osher 1989). Some modifications (described below) were made to the basic scheme to improve the solution accuracy, and to enhance the code performance.

The ENO scheme was first evaluated by computing the spatially decaying compressible turbulence without shocks. The order of the ENO scheme required to reproduce the evolution of turbulence was assessed. During the validation procedure, an unexpected degeneracy in accuracy was observed with the increase in the order of the ENO scheme. Similar degeneracy was reported by Rogerson & Meiberg (1990) when the mesh was refined. This degeneracy was determined to be caused by the use of linearly unstable stencils in the adaptive procedure. Biasing toward a central difference stencil was implemented to avoid the accuracy degeneracy in a shock-free region (Shu 1990). With this modification, more accurate results were obtained with raising the order of accuracy. Results comparable to those obtained with a sixth-order-accurate central Padé scheme was obtained with a sixth-order ENO scheme.

When the ENO scheme is implemented throughout the domain, the operation count and, accordingly the CPU time, increase significantly compared to the Padé scheme. However, the region where the ENO scheme plays a significant role is quite localized. It was usually less than a tenth of the computational domain in our DNS of weak shock waves, and was expected to be even smaller for stronger shock waves. The idea of applying the ENO scheme only where it plays an active role and switching elsewhere to the usual Padé central differencing was therefore tested. Switching to the

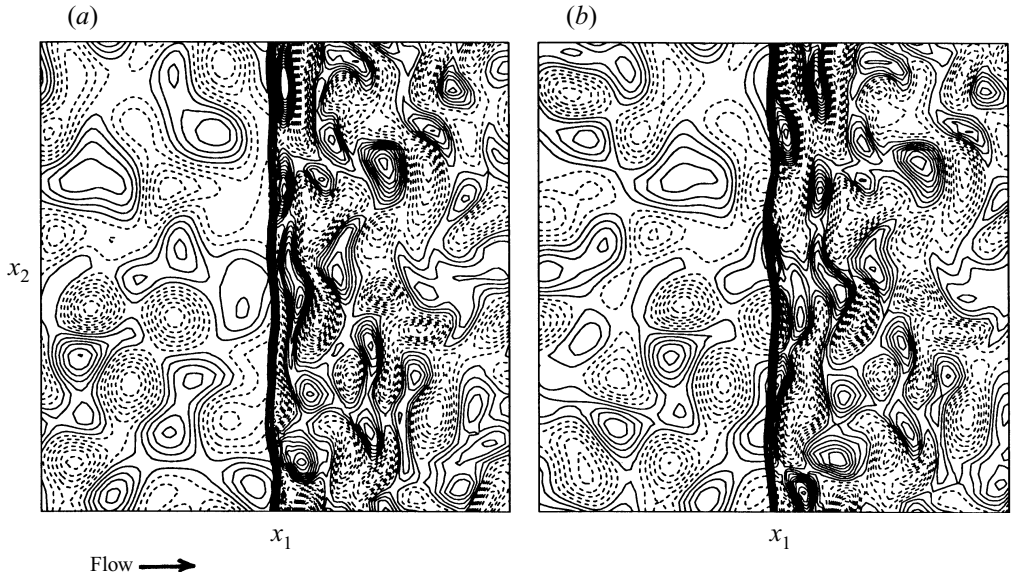

FIGURE 1. Figure 1. Snapshots of vorticity (ω_3) contours in shock/turbulence interaction with $M_1 = 2.0$ at (*a*) $tc/L_1 = 1.951$, (*b*) $tc/L_1 = 2.053$, where L_1 is the computational box size in the x_1-direction: solid lines, $\omega_3 > 0$; dashed lines, $\omega_3 < 0$; Superposed contours near the centre of each plot are constant-dilatation lines, denoting an instantaneous shock location.

Pade scheme beyond the region occupied by the shock is justified *a posteriori* by the smoothness of the computed solution across such transitions. The local region of ENO application can be specified *a priori* to be a zone around the shock for a simulation performed in a coordinate system fixed on the mean shock wave. The concept of local application of the ENO scheme was validated against fully resolved DNS results, both for the case of two-dimensional shock turbulence interaction (Lee *et al.* 1991*a*) with $M_1 = 1.2, M_t = 0.07$ and the case of three-dimensional spatially decaying turbulence (Lee *et al.* 1992*b*) with $M_t = 0.51$ and $Re_\lambda = 25$. Here, $M_1 = \bar{u}_1/\bar{c}, M_t = q/\bar{c}$, and $Re_\lambda = \bar{\rho} u_{rms} \lambda/\bar{\mu}$, where $u_{rms} = (\widetilde{u_1''^2})^{1/2}$, $q^2 = \widetilde{u_i'' u_i''}$, c is the sound speed, λ is a Taylor microscale, and μ is the dynamic viscosity. The overline denotes an ensemble average, and f' and f'' are the deviations from the ensemble average and the mass-weighted average (Favre 1965) $\tilde{f} = \overline{\rho f}/\bar{\rho}$, respectively.

The next validation computation was to reproduce the three-dimensional interaction of turbulence with a weak shock using the ENO scheme. The results were compared to our past shock-resolving computations. Significant additional dissipation of turbulent kinetic energy (TKE) was found in the shock vicinity where the ENO scheme was applied independently in all directions. This dissipation was less pronounced in two-dimensional shock-turbulence simulations. From a numerical point of view, the ENO procedure is a type of upwind difference and has an additional numerical dissipation, or viscosity, in regions of steep gradients. Since steep gradients in turbulent flows occur at small scales the ENO scheme, when applied over the entire flow domain, may give undesirable damping of turbulence. In the present problem the location of the shock is known *a priori* and it is natural to introduce the ENO scheme only in a specific direction (normal to the undisturbed shock) in a zone surrounding the shock wave. Since the change in the shock normal direction due to the unsteady shock distortions is only about 1% as shown by Lee *et al.* (1993), the flow variables do not change

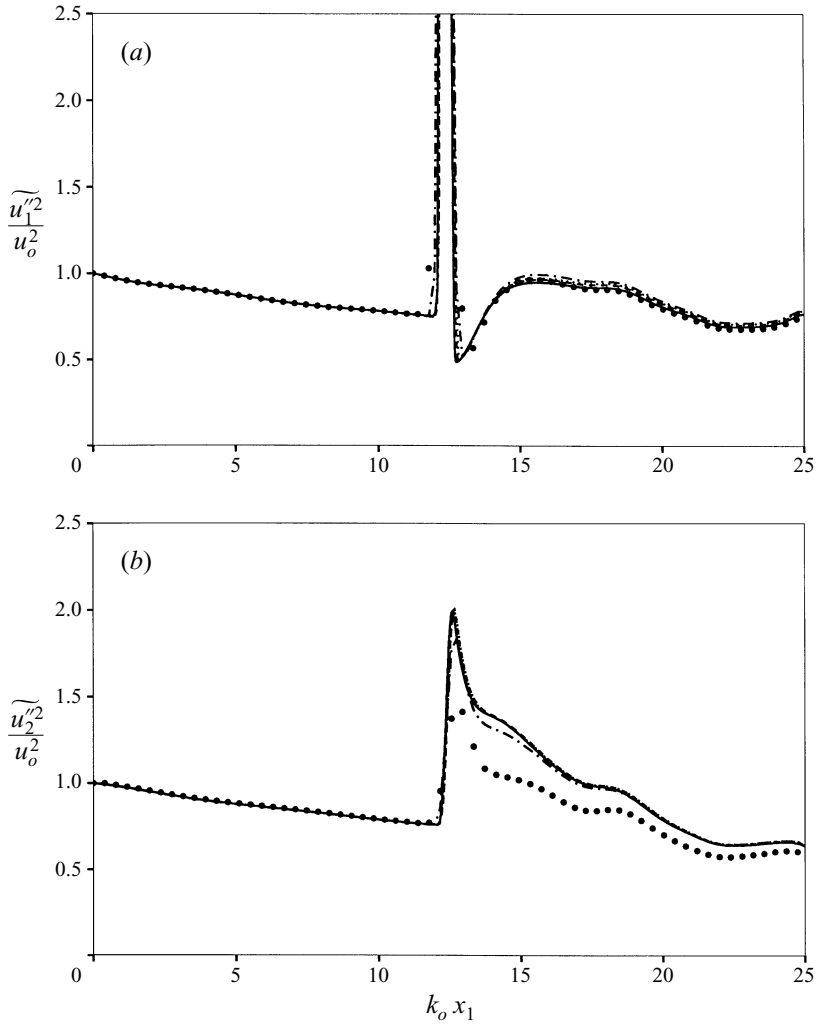

FIGURE 2. Evolution of (*a*) the streamwise and (*b*) the transverse velocity fluctuation variance for different grid resolutions ($M_1 = 2.0, M_t = 0.07$). DNS: ——— , $r_\Delta = 3/160$. ENO: - - - - , $r_\Delta = 3/40$; ····· , $r_\Delta = 1/8$; —·— , $r_\Delta = 3/8$; • , $r_\Delta = 3/4$.

as rapidly in the directions transverse to the shock; one-dimensional application of ENO scheme in the mean shock normal direction is found to be sufficient for shock capturing. This also significantly reduces the computational expenses. For $M_1 = 1.2$, the ENO scheme required only a quarter of the CPU time of the corresponding shock-resolving simulation (Lee 1992).

The final validation calculation was made for two-dimensional turbulence interacting with a strong shock wave. A typical time sequence of vortical structures interacting with the shock wave is shown in figure 1(*a*, *b*), where advection of vortical structures and their interaction with the shock wave are clearly observed. Deformation and amplification of the vortical structures are to be noted as they pass through the shock wave. The evolutions of velocity fluctuation variances is shown in figure 2 for different resolutions near the shock wave. A non-uniform grid was used in the streamwise direction such that points were clustered around the shock, while a uniform grid

was used in the transverse direction. The sixth-order-accurate ENO shock-capturing scheme was activated only at 12 points upstream and 12 points downstream of the mean shock position. This was sufficient in the present simulation to cover the region instantaneously occupied by the shock wave during its unsteady motion. This region was determined by considering the estimate of shock front displacements predicted by LIA (Lee *et al.* 1992*b*). Since the shock wave was always included in the region of ENO application, the interface of scheme transition could not be discerned from the simulation results.

The turbulence at the inflow of the computational domain was generated to have an energy spectrum, $E(k) \simeq u_o^2 (k/k_o)^4 \exp[-2(k/k_o)^2]$, where k_o is the peak wavenumber and u_o is the r.m.s. velocity fluctuation. This spectrum was chosen as a good representation of low-Reynolds-number DNS. The von Kármán spectrum (Hinze 1975)

$$E(k) \simeq u_o^2 \frac{(k/k_o)^4}{\left[1 + (k/k_o)^2\right]^{17/6}}$$

is a better overall approximation for high-Reynolds-number turbulence. Serious resolution problems would have occurred if the von Kármán spectrum had been used at the inflow. This spectrum is used, however, in LIA to better approximate the real turbulence. Turbulence amplification across the shock wave is not dependent on the shape of the upstream spectrum. But the inhomogeneous turbulence evolution downstream of the shock (figure 3*c*) and the one-dimensional spectrum change across the shock (figure 6) are dependent on the shape of the upstream spectrum. Dependency of the LIA predictions on the spectrum shape, when it exists, was found not crucial to the discussions in the present work.

Results from the ENO scheme on two-dimensional shock/turbulence interaction were compared with the corresponding shock-resolving simulation. The inflow conditions were maintained at $M_1 = 2.0$, $M_t = 0.14$, and $k_o = 4$ in all cases. The dynamic viscosity was set to give a Reynolds number $\rho u_o/(\mu k_o) = 16.7$ at the inflow. The computational domain was discretized by a uniform grid of 48 points in the transverse direction and a non-uniform grid was used in the streamwise direction for different shock resolutions for each case. The uniform grid in the transverse directions was fine enough for turbulence resolution. In the shock-capturing simulation, as the streamwise grid is refined near the shock wave the computed results approach the shock-resolving DNS predictions. As the resolution becomes poor, the shock-capturing simulation could not reproduce the evolutions of transverse velocity and entropy fluctuations of the corresponding shock-resolving simulation. The minimum grid spacing required by the ENO scheme was about seven times larger than that used in the shock-resolving simulation.

Shock front corrugation has a leading-order effect on the modification of transverse velocity fluctuations, while it plays a weaker role in shock-normal component modification. Therefore, the evolution of transverse velocity fluctuations cannot be accurately predicted without resolving the corrugation. The shock front inclination angle scales with upstream turbulence intensity, $i_t = u_{rms}/\bar{u}_1$. The shock-normal grid spacing should be refined near the shock wave to yield a grid aspect ratio of $r_\Delta = \Delta x/\Delta y = O(i_t)$ for a shock-resolving (DNS) simulation. In simulations with a shock-capturing scheme, the relevant length scales are shock corrugation length scale and turbulence length scales; shock thickness is irrelevant since the shock wave structure is not resolved but numerically captured. Since the shock corrugation length scale is comparable to the turbulence length scales (Lee 1992) the solution convergence

may be described in terms of the shock front corrugation resolution (r_Δ). Comparable results can be obtained for the shock-capturing simulation (figure 2*a*) with a grid aspect ratio about 7 times larger than necessary in the shock-resolving simulation.

Grid refinement is also necessary to predict thermodynamic fluctuations correctly, since the convergence of the thermodynamic variables is slowest due to spurious numerical oscillations in entropy behind the shock wave (Roberts 1990; Meadows, Caughey & Casper 1993). The spurious oscillations are intrinsic to all the shock-capturing schemes when applied to a slowly moving shock wave, which travels one mesh spacing in more than 20 time steps. Since the present simulations are performed in a coordinate system fixed on the mean shock position, the spurious oscillations may affect the quality of the shock-capturing simulations. It was found that with the same resolution the oscillations are more pronounced for a shock-capturing scheme which gives sharper transitions across the shock wave: more oscillations are observed for the (less dissipative) Roe scheme than the Lax-Friedrichs scheme. For a given shock-capturing scheme, fewer entropy oscillations are noticed for a simulation with the finer grid. Accurate prediction of the interaction of turbulence with a shock wave, where a shock-resolving simulation is not practical, can only be obtained after a thorough grid-refinement test.

The assumptions and numerical procedures used in this paper can be summarized as follows. The fluid is assumed to be an ideal gas with the specific heat ratio, $\gamma = 1.40$. The Prandtl number is assumed constant with $Pr = 0.75$. The density, three components of momentum, and the total energy are advanced in time using a third-order compact-storage Runge–Kutta scheme (Wray 1986). Spatial derivatives are approximated by the sixth-order ENO scheme only for the inviscid fluxes in the mean shock-normal direction and within a zone near the shock wave, and by the sixth-order Padé scheme (Lele 1992) for the other terms and in the other regions. The ENO scheme is activated over 12 grid points upstream and downstream of the mean shock wave, which is found sufficient in all cases studied. The simulation is performed in a coordinate system fixed on the mean shock position, where flow is supersonic upstream and subsonic downstream. The direction of the mean flow was chosen to be normal to the shock wave, which was aligned with the x_1-axis. At the inflow, isotropic turbulence is added to the supersonic mean flow. A 'realistic' turbulence is prescribed at the inflow using a data base from a temporally decaying turbulence (Lee, Lele & Moin 1991*b*). Special care is taken so that turbulence upstream of the shock wave is fully developed with proper velocity derivative skewnesses. A non-reflecting boundary condition (Giles 1990) is applied at the outflow boundary. Periodic boundary conditions are imposed in the transverse directions due to the homogeneity of turbulence in these directions. More details on the numerical schemes can be found in Lee *et al.* (1992*b*).

2.2. *Linear interaction analysis (LIA)*

Some aspects of the interaction of shock waves and turbulence are predictable through linear analysis. For the linear analysis to apply, the upstream fluctuation must be a small-amplitude perturbation to the mean upstream state. Furthermore, the time required for turbulence to pass through the shock wave should be small compared to the turbulence time scale, $\overline{\rho} q^2/\epsilon$ (ϵ is the dissipation rate of turbulence kinetic energy), so that there would be insufficient time for the redistribution of energy into different scales through nonlinear processes.

As a small-amplitude vorticity wave interacts with a shock wave, two other elementary waves – acoustic and entropic waves – are generated behind the shock wave

and the vorticity wave is refracted. Through linear analysis, amplitudes, length scales and orientations of downstream refracted or generated waves can be represented in terms of those of the upstream vorticity wave. In this work, we employed the linear interaction analysis (LIA) of Ribner (1953). In LIA, inviscid linear equations for the disturbances are solved downstream of the shock wave, and the boundary conditions at the downstream side of the shock front are expressed in terms of the upstream disturbances by the use of linearized Rankine–Hugoniot relations.

For an upstream elementary vortical wave with $u^1_\omega(\boldsymbol{x}) = \hat{u}^1_\omega(\boldsymbol{k})\exp(\mathrm{i}\boldsymbol{k}\cdot\boldsymbol{x})$, on solving the appropriate equations the Fourier coefficients of the downstream elementary waves (refracted and generated) can be obtained as

$$\hat{u}^2_\omega(\boldsymbol{k}) = \Pi(\theta; M_1)\hat{u}^1_\omega(\boldsymbol{k}), \quad \hat{p}^2(\boldsymbol{k}) = P(\theta; M_1)\hat{u}^1_\omega(\boldsymbol{k}), \quad \hat{s}^2(\boldsymbol{k}) = \Sigma(\theta; M_1)\hat{u}^1_\omega(\boldsymbol{k}),$$

where u_ω denotes the solenoidal velocity component, $\hat{f}$ the Fourier coefficient of f, and superscripts ^{1} and ^{2} denote upstream and downstream conditions, respectively. The transfer functions Π, P and Σ are functions of upstream mean Mach number and the angle of incidence (θ) of the elementary wave. Their detailed expressions may be found in Ribner (1953). In the near field, they also depend on the distance from the shock wave. However, significant near-field effects occur only within a distance of one wave length downstream of the shock wave, as is shown in figure 3(c). The transfer functions carry information not only about amplitudes but also about propagation directions for the far-field downstream waves. Therefore, downstream elementary vortical, acoustic, and entropy waves can be obtained for each upstream elementary wave. Velocity fluctuations associated with acoustic waves can be obtained assuming linear acoustic wave propagation, and other thermodynamic fluctuations can be derived from the pressure and entropy fluctuations.

Since upstream turbulence may be approximated as a superposition of vorticity waves, modification of turbulence through the shock can be predicted via LIA (Ribner 1954, 1987) by adding up the contributions of the downstream elementary waves. Modifications of some turbulence statistics previously reported (Ribner 1987; Lee *et al.* 1993) are reproduced in the present paper for completeness.

3. Results and discussion

The primary parameters in the simulation are the mean Mach number (M_1), the fluctuation Mach number (M_t), and the turbulence Reynolds number based on the Taylor microscale (Re_λ) upstream of the shock wave. In the simulation, all turbulence scales are fully resolved, while the effect of the shock wave on turbulence is captured (rather than fully resolved). Three simulations with $M_1 = 1.5, 2.0$ and 3.0 are conducted for the interaction with strong shock waves, and the results from shock-resolving simulations (Lee *et al.* 1993) for the interaction with a weak shock wave ($M_1 = 1.05, 1.1, 1.2$) are quoted for comparison. Since the shock wave thickness is not meaningful in a linear analysis and in a shock-capturing simulation, turbulence length scales are the only physical length scales. In discussing the results from the simulation the turbulence length scale measure (k_o^{-1}) is used as the reference length scale. Table 1 lists the simulation parameters, where the values of M_t and Re_λ are taken at the location immediately upstream of the shock.

3.1. *Velocity fluctuations*

The interaction of turbulence with a shock wave generates acoustic waves downstream of the shock, some of which undergo rapid decay (Ribner 1953). LIA predicts that

Case	M_1	M_t	Re_λ	k_o
A	1.5	0.0897	15.7	4.0
B	2.0	0.108	19.0	4.0
C	3.0	0.110	19.7	4.0

TABLE 1. Simulation parameters

turbulent kinetic energy is amplified across the shock wave and the evanascent acoustic waves contribute significantly to the streamwise fluctuations just behind the shock wave. Figure 3(*a*) shows the evolution of the diagonal components of the Reynolds stress tensor, $R_{ij} = \widetilde{u_i'' u_j''}$. The off-diagonal components (not shown) stay close to zero over the entire flow field since turbulence is isotropic upstream and axisymmetric downstream of the shock. The streamwise component of turbulence intensity in the shock region contains the intermittency effects due to the oscillations of the shock (for more details on the intermittency effects on turbulence statistics, see Lee *et al.* 1992*b*). The boundaries of the shock oscillations are defined as the locations where mean dilatation $\mathrm{d}\bar{u}_1/\mathrm{d}x_1 = 0$; $\mathrm{d}\bar{u}_1/\mathrm{d}x_1$ is negative inside the shock wave and slightly positive away from the shock due to viscous heating. All components of the velocity fluctuations are enhanced during the interaction. The velocity fluctuations are axisymmetric behind the shock, and their return to isotropy is negligible compared to the decay. Due to the evanescent acoustic waves the velocity fluctuations evolve rapidly just downstream of the shock wave. Away from the shock wave, however, all the velocity fluctuations decay monotonically due to viscous dissipation.

The Mach number dependence of the far-field velocity fluctuation amplification predicted by LIA is shown in figure 3(*b*). All components of the velocity fluctuation are amplified across the shock wave, and the amplification of TKE tends to saturate beyond $M_1 = 3.0$. The shock-normal component is amplified more for shock waves with $M_1 < 2.0$ while the opposite is true for $M_1 > 2.0$. In DNS, the streamwise velocity fluctuation away from the shock is larger than the transverse velocity fluctuations, which seemingly contradicts the LIA prediction. However, comparing low-Reynolds-number DNS results directly with the inviscid linear analysis may not be appropriate. The inviscid terms in the TKE transport equation are dominant only in the region immediately downstream of the shock wave, beyond which the viscous terms are significant (Lee *et al.* 1993). The monotonic viscous decay rate of the transverse components are found to be significantly higher than that of the streamwise component. After the viscous decay is compensated for by extrapolating the downstream monotonic decay back to the shock location, the DNS results are found to be consistent with the LIA prediction.

The rapid downstream evolution of velocity fluctuations which was observed for weak shock/turbulence interaction (Lee *et al.* 1992*b*) persists in the present simulations with stronger shocks. The evolution of the velocity fluctuations downstream of the shock wave predicted by LIA is shown in figure 3(*c*), which reproduces the main feature of the rapid evolution from the DNS. Hence, the rapid TKE evolution behind the shock wave can be explained mainly as a linear process. This rapid evolution in the streamwise velocity fluctuation is due to a correlation between the vortical and evanescent acoustic fluctuations behind the shock wave. The acoustic velocity fluctuations and vortical velocity fluctuations are anti-correlated just behind the shock, and the correlation between the two fluctuations decreases rapidly as the amplitude

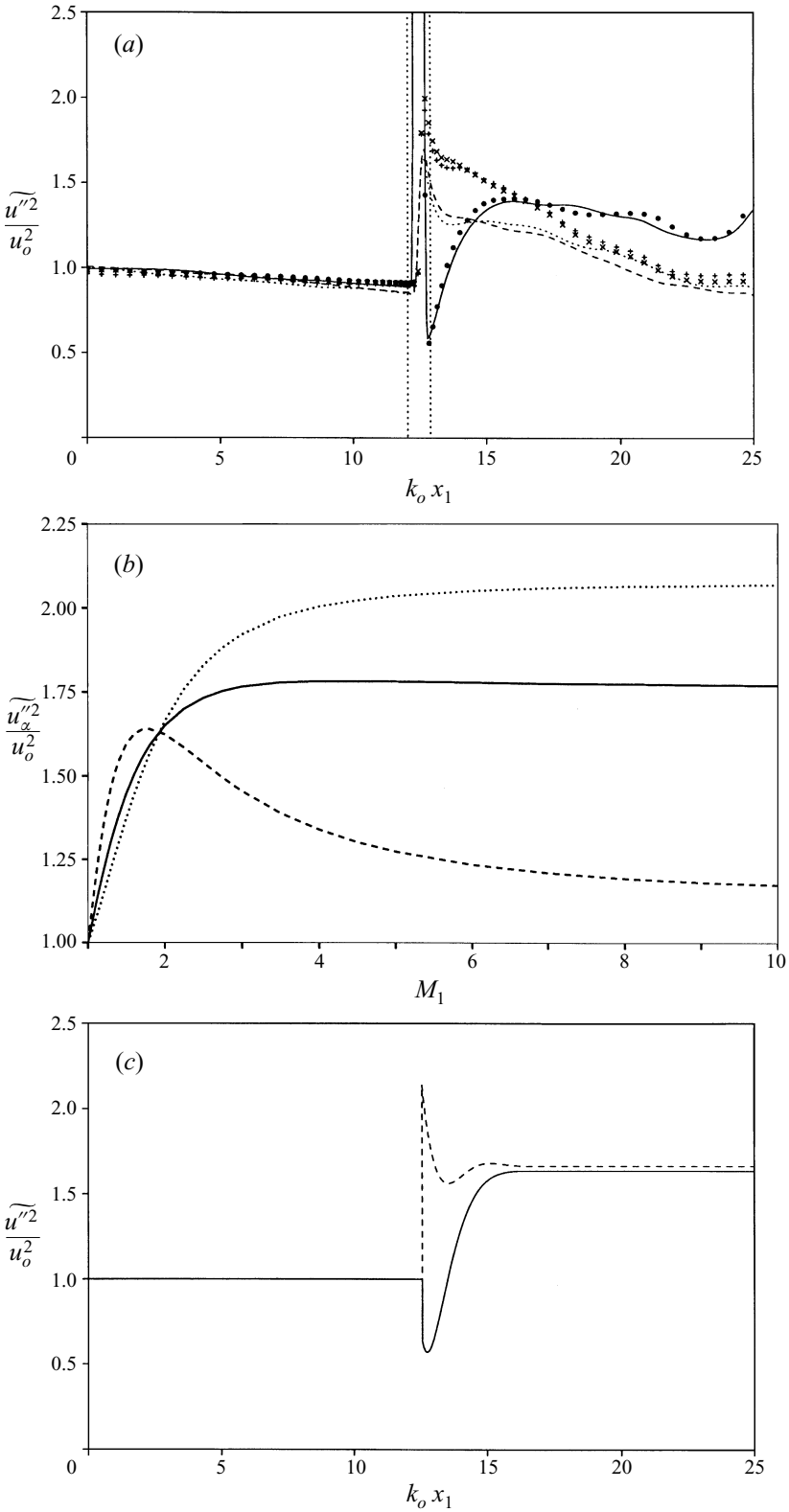

FIGURE 3. For caption see facing page.

of the acoustic wave decays exponentially away from the shock wave. In previous studies (Lee *et al.* 1991*a*, 1992*a*, 1993), the correlations between vortical and acoustic waves were not properly accounted for, and the prediction capability of the linear analysis was not fully appreciated.

Further insight into the rapid evolution of velocity fluctuations is revealed by the equation for energy balance satisfied by linearized disturbances (e.g. Thompson 1985). The continuity and momentum equations for the linearized fluctuating components can be written as

$$\frac{\partial \rho'}{\partial t} + \widetilde{u}_k \frac{\partial \rho'}{\partial x_k} + \overline{\rho} \frac{\partial u_k''}{\partial x_k} = 0,$$

$$\frac{\partial u_i''}{\partial t} + \widetilde{u}_k \frac{\partial u_i''}{\partial x_k} + \frac{1}{\overline{\rho}} \frac{\partial p'}{\partial x_i} - \frac{\partial \sigma_{ik}''}{\partial x_k} = 0$$

by assuming that there exist no mean flow gradients, where $\overline{\rho}\sigma_{ij}''(=\tau_{ij}'')$ denotes the viscous stress. For an ideal gas the linearized equation of state gives the density fluctuation in terms of the pressure and entropy (s) fluctuations as

$$\frac{\rho'}{\overline{\rho}} = \frac{1}{\gamma}\frac{p'}{\overline{p}} - \frac{s'}{c_p}, \tag{1}$$

where c_p is the specific heat at constant pressure. Multiplying the continuity equation by ρ', contracting the momentum equations by u_i'', and cancelling density–dilatation correlation by using the above thermodynamic relation and neglecting the entropy fluctuation effect ($-\overline{s'u_{i,i}''}/c_p\overline{c}$), gives the following equation (in the averaged form):

$$\frac{\partial}{\partial x_1}\left[\frac{\widetilde{u}_1}{\overline{c}}\left(\frac{\overline{u_i''u_i''}}{2\overline{c}^2} + \frac{\overline{\rho'^2}}{2\overline{\rho}^2}\right) + \frac{1}{\gamma}\frac{\overline{p'u_1''}}{\overline{p}\,\overline{c}}\right] - \frac{\overline{u_i''}}{\overline{c}^3}\frac{\partial \sigma_{ik}''}{\partial x_k} = 0.$$

With this relation, the rapid post-shock evolution noted earlier in figure 3(*a*) can be explained in terms of the energy balance for linearized disturbances. Entropy and acoustic (or dilatation) modes are perfectly decorrelated for small-amplitude fluctuations (Kovásznay 1953) in the linear limit. The DNS data shown in figure 4(*a*) confirm that the correlation between the entropy fluctuations and dilatation decays rapidly downstream of the shock and its maximum contribution to the energy balance is less than 5% of the pressure transport term.

The energy balance equation integrated in the streamwise direction from a location (x_s) downstream of the shock up to a location (x) further downstream gives

$$\underbrace{\left\|\frac{\widetilde{u}_1}{\overline{c}}\frac{\overline{u_i''u_i''}}{2\overline{c}^2}\right\|_{x_s}^{x_1}}_{A} + \underbrace{\left\|\frac{\widetilde{u}_1}{\overline{c}}\frac{\overline{\rho'^2}}{2\overline{\rho}^2}\right\|_{x_s}^{x_1}}_{B} + \underbrace{\left\|\frac{1}{\gamma}\frac{\overline{p'u_1''}}{\overline{p}\,\overline{c}}\right\|_{x_s}^{x_1}}_{C} \underbrace{- \int_{x_s}^{x_1} \frac{\overline{u_i''}}{\overline{c}^3}\frac{\partial \sigma_{ik}''}{\partial x_k}\mathrm{d}x_1}_{D} = 0,$$

where $\|f\|_a^b = f(b) - f(a)$. Terms labelled in this equation are shown in figure 4(b). In

FIGURE 3. (*a*) Evolution of the normal components of the Reynolds stress: lines for $M_1 = 2.0$, and symbols for $M_1 = 3.0$. ——— , • , R_{11}; – – – – , × , R_{22}; ····· , + , R_{33}. Vertical lines denote the boundaries of shock intermittency. (*b*) Amplification of velocity fluctuation variances across the shock wave predicted by LIA far away from the shock. ——— , q^2/q_o^2; – – – – , $\widetilde{u_1''^2}$; ····· , $\widetilde{u_2''^2}$, $\widetilde{u_3''^2}$. (*c*) Evolution of velocity fluctuation variances behind the shock wave predicted by LIA ($M_1 = 2.0$) using the spectrum with exponential fall-off used in the DNS. ——— , $\widetilde{u_1''^2}$; – – – – , $\widetilde{u_2''^2}$, $\widetilde{u_3''^2}$.

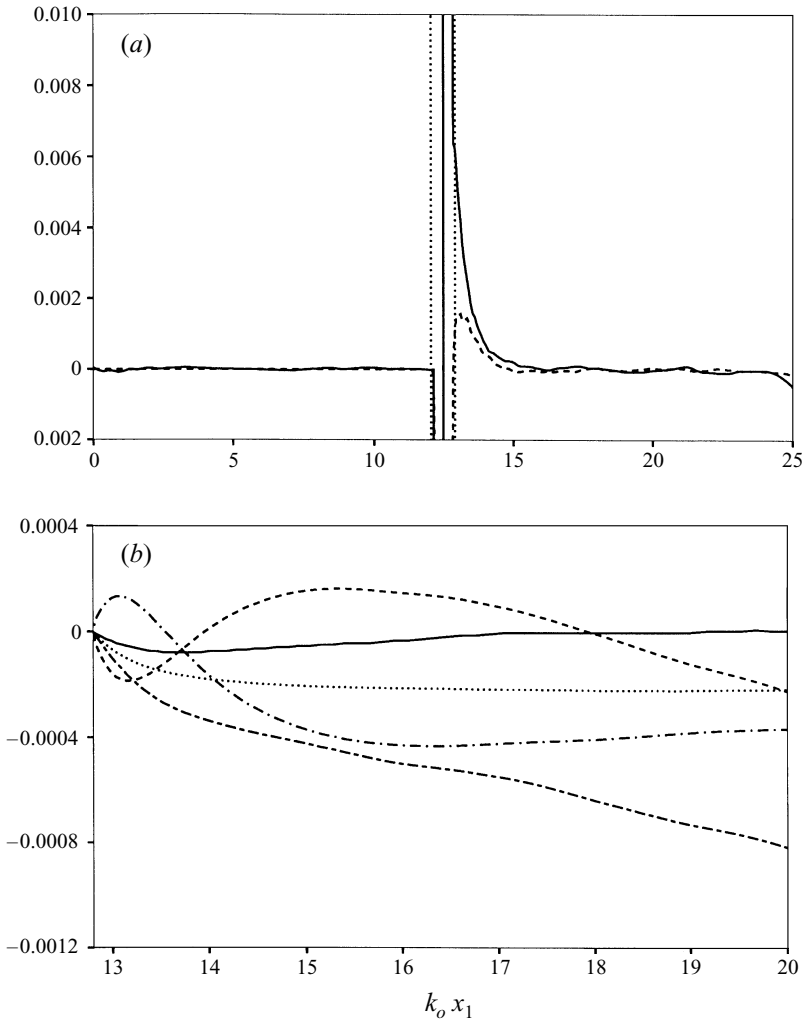

FIGURE 4. (*a*) Evolution of pressure–dilatation correlation and entropy–dilatation correlation for $M_1 = 2.0$: ——— , $\overline{p' u''_{k,k}}/\gamma \bar{p} u_o k_o$; - - - - , $-\overline{s' u''_{k,k}}/c_p u_o k_o$. Vertical lines denote the boundaries of shock intermittency. (*b*) Evolution of the integrated quantities from the acoustic energy balance for $M_1 = 2.0$: - - - - , A; ····· , B; —·— , C; —·· , $A + B + C$; ——— , $A + B + C + D$.

all the cases we investigated (with different shock strengths and upstream turbulence intensities) the energy budget is balanced with little deviation. The sum of scaled density and velocity fluctuations is found to be mainly compensated by the pressure transport. Therefore, the rapid evolution of velocity fluctuations can be attributed to an energy transfer from the acoustic potential energy in the form of density (or pressure) fluctuations to turbulent kinetic energy through the pressure transport. The pressure-transport term also scaled best by flow variables associated with acoustic fluctuations (Lee *et al.* 1993).

Variance of vorticity fluctuations is the main contributor to the TKE dissipation rate. Figure 5(*a*) shows the evolution of vorticity components. The transverse components are amplified across the shock, while the streamwise component is hardly affected. Downstream of the shock the streamwise vorticity fluctuations increase. This

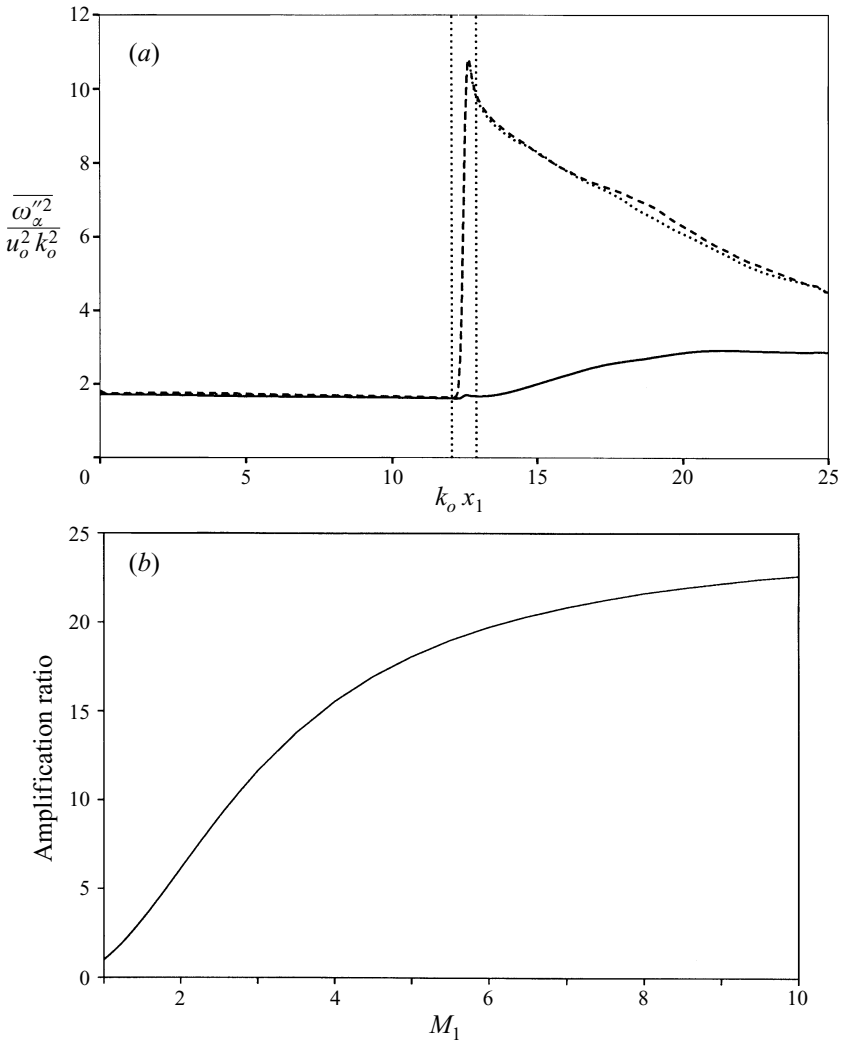

FIGURE 5. (*a*) Evolution of the vorticity fluctuation variances ($M_1 = 2.0$): ——— , $\overline{\omega_1'^2}$; - - - - , $\overline{\omega_2'^2}$; ····· , $\overline{\omega_3'^2}$. (*b*) Amplification of transverse vorticity fluctuation variances predicted by LIA.

is a nonlinear process occurring as the intensified vorticity in the x_2- and x_3-directions is tilted and stretched by turbulent fluctuations. The Mach number dependence of transverse vorticity variance amplification is shown in figure 5(*b*). LIA predicts no amplification of the streamwise component. Vorticity is amplified more for the stronger shock wave, and the amplification saturates rather slowly compared to the TKE amplification (figure 3*b*). The amplification ratios obtained from DNS are found to be consistent with the LIA predictions to within 5%.

3.2. *Turbulence length scales*

Experimental studies (Honkan & Andreopoulos 1992; Debieve & Lacharme 1986; Keller & Merzkirch 1990) have reported that large-scale turbulent motions are enhanced more than small-scale motions as turbulence passes through a shock wave, leading to the overall increase of turbulence length scales, especially of microscales.

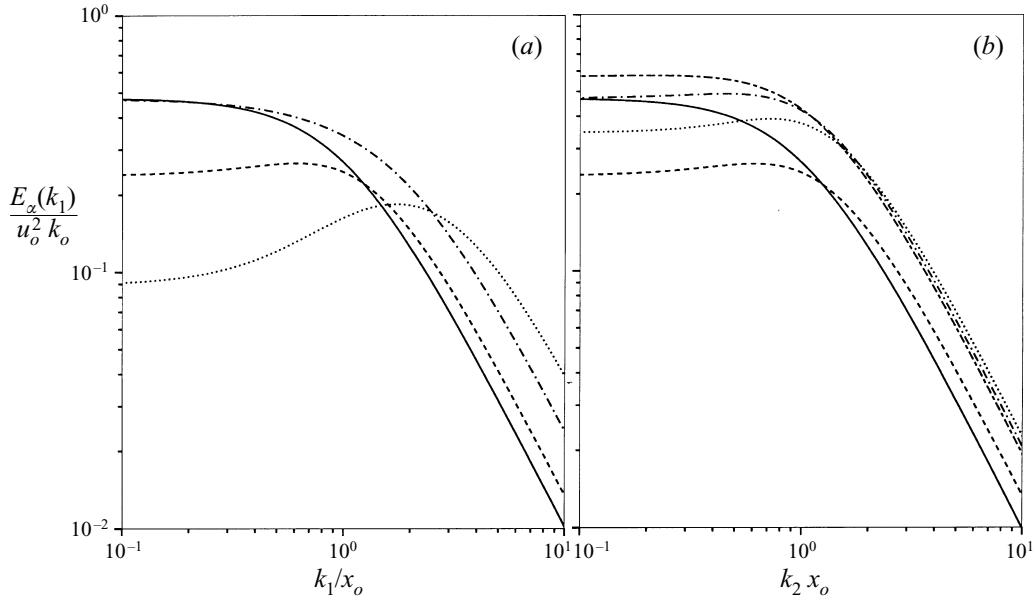

FIGURE 6. LIA prediction of one-dimensional energy spectra changes across the shock wave for (*a*) $M_1 = 2.0$ vs. k_1. E_1: ——— , upstream; —·— , downstream. E_2, E_3: – – – – , upstream; ····· , downstream. (*b*) $M_1 = 2.0$ vs. k_2. E_2: ——— , upstream; —·— , downstream. E_1: – – – – , upstream; ····· , downstream; E_3: – – – – , upstream; —– —, downstream.

However, LIA predicts that Taylor microscales decrease across the shock wave for all shock strengths, which was confirmed by DNS for weak shock waves (Lee *et al.* 1991*a*, 1993). For weak shock waves, changes in some turbulence length scales were too small to provide definite trends.

To investigate the scale-dependent amplification of turbulence, the modification of power spectra across the shock wave ($M_1 = 2.0$) is computed by LIA for the one-dimensional far-field energy spectrum in the shock-normal (longitudinal) and transverse directions which are shown in figure 6. The spectrum, $E_\alpha(k_\beta)$, is defined as the spectral energy density of $\overline{u_\alpha'^2}$ at k_β, where k_β is the wavenumber in the x_β-direction, so that

$$\overline{u_\alpha'^2} = \int_0^\infty E_\alpha(k_\beta)\mathrm{d}k_\beta.$$

In the longitudinal spectra, significant scale-dependent amplification is observed: more amplification at small scales than at large scales. The large-scale part of $E_2(k_1)$ is even suppressed through the interaction. In the transverse spectra, more amplification at small scales is found for $E_1(k_2)$ and $E_2(k_2)$, while more amplification at large scales is found for $E_3(k_2)$. Since the amplification pattern is different for different spectra (e.g. $E_1(k_2)$ or $E_3(k_2)$), the issue of length scale change should be addressed separately for each specific length scale. In the following, changes in various turbulence length scales are discussed.

Transverse spectra of velocity fluctuations in the numerically simulated field for $M_1 = 2.0$ are shown for upstream and downstream of the shock wave in figure 7. The amplification is more pronounced at the large wavenumbers, which is consistent with the prediction by the linear analysis in figure 6(*b*). More direct comparison could not

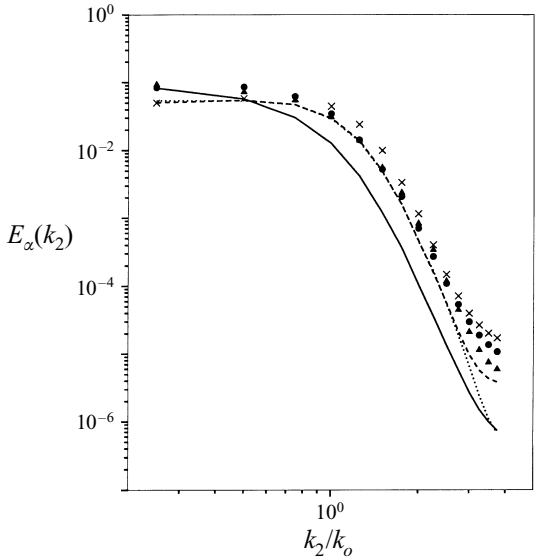

FIGURE 7. Changes in one-dimensional spectra across the shock wave which is at $k_o x_s = 12.29$: lines for upstream spectra at $k_o x_1 = 10.59$, and symbols for downstream spectra at $k_o x_1 = 13.68$. ——— , • , $E_2(k_2)$; – – – – , × , $E_1(k_2)$; ····· , ▲, $E_3(k_2)$.

be made since the inflow turbulence spectrum used in the simulation is different from the one used in LIA.

Keller & Merzkirch (1990) reported that both the integral length scale based on density fluctuations and the density microscale in a transverse direction increase for shock waves with $M_1 < 1.24$. In the present simulation, the spectral changes of density and temperature fluctuations across the shock are found to be similar to those of velocity fluctuations: spectra are amplified more at small scales than at large scales. The experimental study of Keller & Merzkirch (1990) invokes the assumptions of turbulence isotropy/homogeneity and negligible pressure fluctuations for data analysis, whose validity is in doubt. The present simulations show that the velocity fluctuation variances are axisymmetric (downstream of the shock) as shown in §3.1, and thermodynamic property fluctuations are not isobaric and decay rapidly behind the shock wave as shown in §3.3. The effect of these assumptions on the experimental results has not been investigated and it seems unlikely that they would cause an erroneous increase in the measured microscales.

The auto-correlation of a turbulence quantity f' in the x_2-direction, $C_f(r; x_1)$, is defined as

$$C_f(r; x_1) = \frac{\overline{f'(x_1, x_2, x_3, t) f'(x_1, x_2 + r, x_3, t)}}{\overline{f'^2(x_1, x_2, x_3, t)}},$$

where the average is taken over time and homogeneous directions (x_2- and x_3-directions). The integral scale (Λ_f) is, then, defined as

$$\Lambda_f(x_1) = \int_0^\infty C_f(r; x_1) \mathrm{d}r,$$

where the upper limit of the integration is replaced by $L/2$ when dealing with a numerically simulated field with L being the computational box size in the x_2-direction, where a periodic boundary condition is enforced. Figure 8 shows the

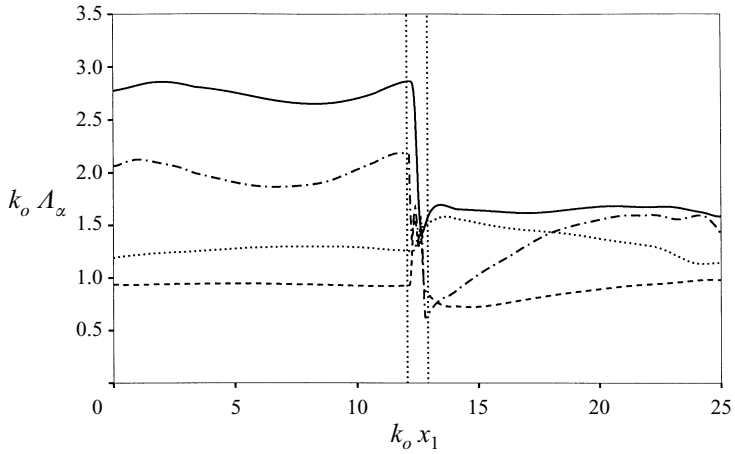

FIGURE 8. Evolution of integral scales throughout the computational domain for $M_1 = 2.0$: ——— , Λ_{u_2}; - - - - , Λ_{u_1}; ····· , Λ_{u_3}; —·—, Λ_ρ. Vertical lines denote the boundaries of shock intermittency.

evolution of four integral scales in the transverse direction throughout the flow field. Three integral scales ($\Lambda_{u_1}, \Lambda_{u_2}$, and Λ_ρ) undergo reductions across the shock wave, most significantly in Λ_{u_2} by about 45%, while Λ_{u_3} increases across the shock by about 30%. Mach number dependence of the integral length scale change was predicted by LIA. For the shock wave with $M_1 = 2.0$, the ratio of the downstream to the upstream integral length scale (with the von Kármán upstream spectrum) is 0.91, 0.60, 1.46 for $\Lambda_{u_1}, \Lambda_{u_2}$, and Λ_{u_3}, respectively. The simulation results agree well with the LIA predictions considering the difference in the upstream energy spectrum shape. (Integral length scales are spectra-dependent.)

Figure 9(*a*) shows the evolution of Taylor microscales (λ_α) and the transverse density microscale (λ_ρ), which are defined as

$$\lambda_\alpha = \frac{(\overline{u'^2_\alpha})^{1/2}}{(\overline{u'^2_{\alpha,\alpha}})^{1/2}} \qquad \text{and} \qquad \lambda_\rho = \frac{(\overline{\rho'^2})^{1/2}}{(\overline{\rho'^2_{,2}})^{1/2}},$$

respectively. All the microscales decrease significantly across the shock wave: the streamwise Taylor microscale by about 50%, the transverse Taylor microscales by about 20%, and the density microscale by about 30%. The Mach number dependence of Taylor microscale changes predicted by LIA are shown in figure 9(*b*). The higher the Mach number, the larger is the reduction of the Taylor microscales through the shock wave. The reduction is more pronounced in the shock-normal direction. The reductions observed in the simulation agree well with the LIA prediction. The experimental result indicating a Taylor microscale increase (Debieve & Lacharme 1986) referred to time scale, not length scale (J. F. Debieve 1992, personal communication). If the mean velocity decrease across the shock is properly accounted for in the use of Taylor's hypothesis, these experimental results are found to be consistent with the present simulation and analysis.

The most widely used length scale in turbulence modelling is the dissipation length scale (l_ϵ), defined as

$$l_\epsilon = \overline{\rho} q^3 / \epsilon,$$

where ϵ is the dissipation rate of turbulence kinetic energy, which includes contribu-

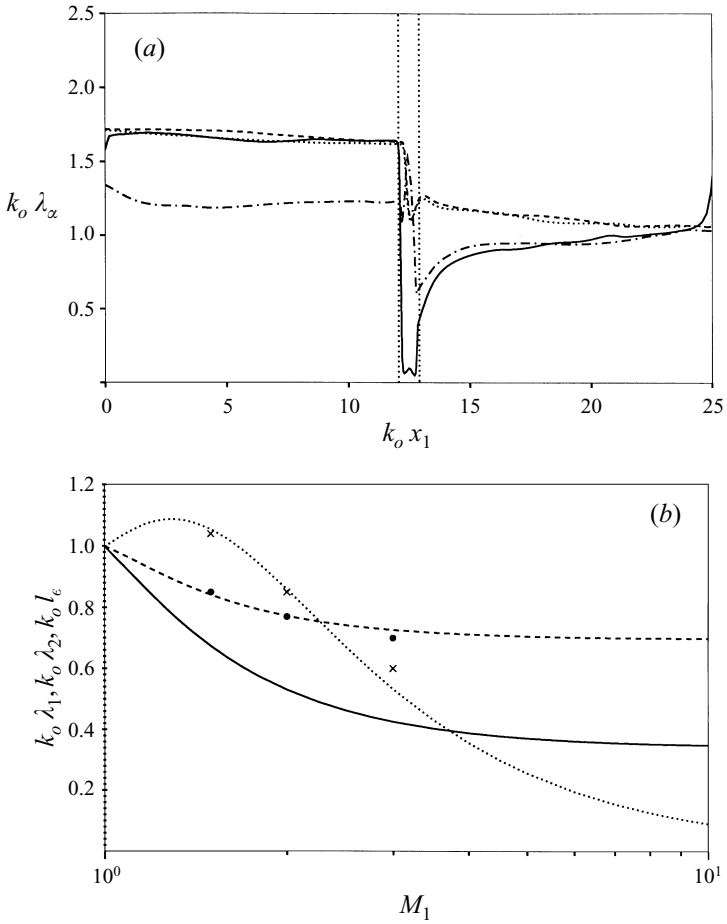

FIGURE 9. (*a*) Evolution of microscales throughout the computational domain for $M_1 = 2.0$: ——— , λ_1; – – – – , λ_2; ····· , λ_3; —·— , λ_ρ. Vertical lines denote the boundaries of shock intermittency. (*b*) Changes of Taylor microscales and dissipation length scale across the shock wave predicted by LIA. ——— , λ_1; – – – – , λ_2, λ_3; ····· , l_ϵ. Symbols for DNS: • , λ_2; × , l_ϵ.

tions from both solenoidal and dilatational motions. Figure 10 shows the evolution of the dissipation length scale. The dissipation length scale also decreases across the shock wave. Just behind the shock wave, l_ϵ undergoes a rapid increase similar to the streamwise Taylor microscale (figure 9*a*), due to the rapid decay of the acoustic waves (or the dilatational motions). The Mach number dependence of the dissipation length scale change predicted by LIA is presented in figure 9(*b*). The length scale is reduced for stronger shock waves, while it shows a mild increase for shock waves with $M_1 < 1.65$. For weak shock waves, TKE and its dissipation rate are comparably amplified to give a slight increase in l_ϵ across the shock wave, while at higher Mach numbers TKE amplification saturates much faster than vorticity variance amplification to give the reduction in the length scale (see figures 3*b* and 5*b*). The dissipation length scale increase observed by Honkan & Andreopoulos (1992) at $M_1 = 1.24$ (the equivalent shock normal Mach number in their experiment is 1.24 mistakenly reported as 1.62) might be explained as the phenomenon occurring for weak shock waves. However, the experimental results are not in quantitative agreement with the

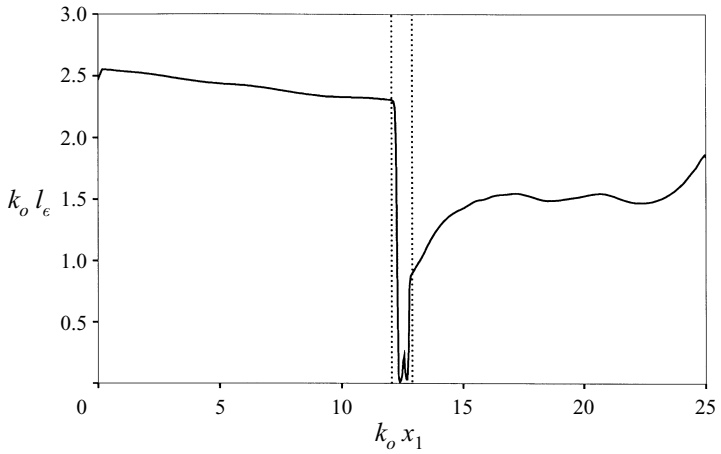

FIGURE 10. Evolution of the dissipation length scale (l_ϵ) throughout the computational domain for $M_1 = 3.0$. Vertical lines denote the boundaries of shock intermittency.

simulation and analysis: LIA predicts less than 10% increase, while the experimental data show more than 600% increase. We know that neglecting pressure fluctuations and application of Taylor's hypothesis in high-intensity turbulence are not in accordance with DNS results. Behind the shock wave, the turbulence intensity level was as high as 25% with large pressure fluctuations; under these conditions Taylor's hypothesis is no longer applicable (Lee *et al.* 1992*a*). Furthermore, the presence of significant upstream pressure fluctuations in the experiment would have an effect on the differences in turbulence modification (Hannappel & Friedrich 1994; Mahesh *et al.* 1995). However, it is unlikely that these assumptions explain the large discrepancies between simulations and experiments.

The experiments conducted so far are not accurate enough to be compared with the simulations, and more refined experiments are planned (J. Keller 1993; J. Andreopoulos 1994, personal communications). Very recently results from new experiments on the interaction of quasi-homogeneous turbulence with a normal shock wave at $M_1 = 3$ have been reported by Barre *et al.* (1996). A multi-nozzle array of 625 (25 by 25) small Mach 3 nozzles was used in the experiment to generate quasi-homogeneous turbulence, and the normal shock was generated by the Mach reflection between the oblique shocks generated by a pair of wedges placed in the flow. Turbulence amplification in rough accord with Ribner's theory and the axisymmetric nature of the turbulence downstream of the interaction zone were noted. The experiment also showed that the longitudinal integral length scale decreased by a factor close to 7 across the shock and the lateral integral scale was unaffected. These trends are in qualitative agreement with those found in the present paper. However, the rather large length scale reduction which exceeds the density ratio (3.8 at $M_1 = 3$) casts some doubts on the quantitative accuracy of the measurements.

3.3. *Thermodynamic quantities*

Thermodynamic fields which are obtained in freely decaying turbulence (Lee *et al.* 1991*b*) and prescribed at the inflow of the present calculations are nearly isentropic. As the flow passes through the shock wave, all the fluctuations are amplified, followed by decay. A polytropic assumption is generally used for the relation between

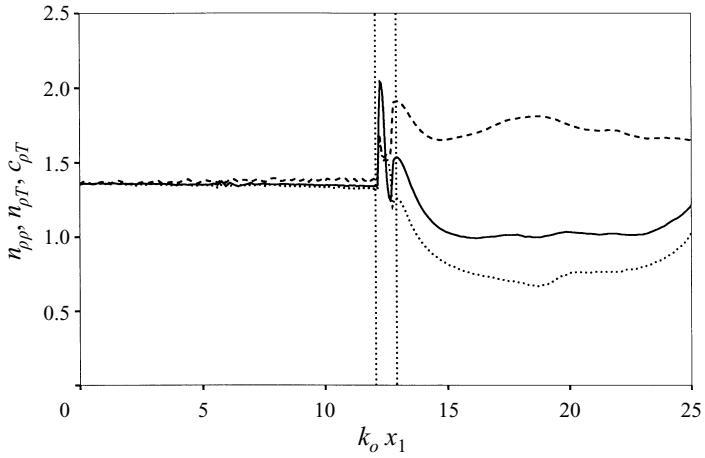

FIGURE 11. Evolution of exponents for the fluctuations in thermodynamic variables for $M_1 = 2.0$: ——— , $n_{p\rho}$; – – – – , $n_{\rho T}$; ····· , $c_{\rho T}$. Vertical lines denote the boundaries of shock intermittency.

thermodynamic fluctuations

$$\frac{p'}{\overline{p}} = n\frac{\rho'}{\overline{\rho}} = \frac{n}{n-1}\frac{T''}{\widetilde{T}},$$

where n is the polytropic exponent. For polytropic fluctuations, specification of one property fluctuation and the polytropic exponent is sufficient to describe all the thermodynamic fluctuations. Based on the above relations, different polytropic exponents can be defined using normalized r.m.s. fluctuations $(n_{p\rho}, n_{\rho T})$ and the correlations between instantaneous fluctuations $(c_{\rho T})$ as

$$n_{p\rho} = \frac{(\overline{p'^2})^{1/2}/\overline{p}}{(\overline{\rho'^2})^{1/2}/\overline{\rho}}, \qquad n_{\rho T} = 1 + \frac{(\overline{T'^2})^{1/2}/\overline{T}}{(\overline{\rho'^2})^{1/2}/\overline{\rho}},$$

and

$$c_{\rho T} = 1 + \frac{\overline{\rho}}{\widetilde{T}}\frac{\overline{\rho' T''}}{\overline{\rho'^2}}.$$

For weak shock waves with $M_1 \leqslant 1.20$, thermodynamic property fluctuations are close to isentropic $(n = \gamma)$ throughout the flow field (Lee *et al.* 1993; Rusak & Cole 1993).

The polytropic exponents, $n_{p\rho}$ and $n_{\rho T}$, are plotted in figure 11. If the fluctuations are indeed polytropic, the two exponents should be the same. This is observed upstream of the shock wave with $n_{p\rho} = n_{\rho T} \simeq \gamma$. Downstream of the shock wave, however, they differ significantly with $n_{p\rho}$ decreasing and $n_{\rho T}$ increasing. Their return to polytropy is very slow. The evolution of $c_{\rho T}$ is also shown in figure 11. Upstream of the shock wave, it is nearly equal to $\gamma(= 1.40)$. It drops significantly across the shock wave, and its further evolution is rather slow. The changes in the exponents across the shock wave are found to be consistent with the LIA prediction (shown in figure 12). Upstream thermodynamic fluctuations are polytropic (close to isentropic), and downstream fluctuations are not isentropic due to significant entropy fluctuations produced by the shock/turbulence interaction. To properly describe the thermodynamic fluctuations in strong shock/turbulence interaction, specification of at least one thermodynamic fluctuation along with two exponents (i.e. $n_{p\rho}$ and $n_{\rho T}$) are required.

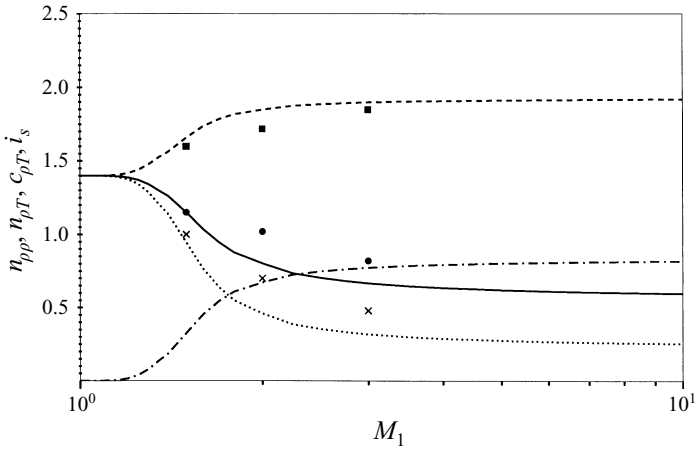

FIGURE 12. Downstream polytropic exponents and entropy fluctuation contribution predicted by LIA. ——— , $n_{p\rho}$; – – – – , $n_{\rho T}$; ····· , $c_{\rho T}$; —·— , entropy fluctuation contribution (i_s). Symbols for DNS: • , $n_{p\rho}$; ■, $n_{\rho T}$; × , $c_{\rho T}$.

The effect of shock strength on thermodynamic fluctuations for a wider range of shock normal Mach numbers can be easily investigated through the linear analysis. In the following, polytropic exponents downstream of the shock in the interaction of solenoidal velocity fluctuations with a shock wave are examined. The effects of the shock strength on downstream polytropic exponents are shown in figure 12. For isentropic or acoustic fluctuations, all exponents are the same and equal to the specific heat ratio. For entropic or isobaric fluctuations, $n_{p\rho}$ and $c_{\rho T}$ become 0 and $n_{\rho T}$ becomes 2. For weak shock waves with $M_1 < 1.2$, thermodynamic fluctuations behind the shock can be regarded as isentropic. As the shock becomes stronger, the entropy fluctuations behind the shock cannot be neglected, and their importance increases for stronger shock waves. The results of the polytropic exponents from DNS are consistent with LIA predictions, with the values from DNS systematically deviating from the LIA predictions toward the isentropic value of 1.4. This may be due to 'incompressible' pressure fluctuations associated with dilatation-free velocity fluctuations (Sarkar *et al.* 1991), with accompanying (approximately isentropic) fluctuations in other thermodynamic quantities.

In order to quantify the significance of entropy fluctuations behind the shock wave, the contribution of entropic fluctuations to the density fluctuations by the linear analysis is shown in figure 12. Since the acoustic fluctuations and entropic fluctuations are completely decorrelated in the linear limit, the relative significance of entropy fluctuations (i_s) can be expressed as

$$i_s = \frac{\overline{s'^2}/c_p^2}{\overline{\rho'^2}/\overline{\rho}^2}$$

using equation (1). For weak shock waves with $M_1 < 1.2$, entropy fluctuations contribute less than 2% to the density fluctuations. However, entropy fluctuations become more significant than acoustic fluctuations beyond $M_1 = 1.65$.

In summary, thermodynamic fluctuations downstream of the shock wave are found to be isentropic for weak shock waves ($M_1 < 1.2$) and become non-polytropic for stronger shock waves, where the importance of entropy fluctuations is comparable to

that of the acoustic fluctuations. The thermodynamic fluctuations cannot be modelled using a single polytropic exponent in this regime. Therefore, acoustic and entropic fluctuations should be modelled separately. Zeman (1993) stressed the need for such a separation for the mean thermodynamic quantities.

4. Conclusion

A shock-capturing scheme is developed for the simulation of the interaction of isotropic turbulence with shock waves. A modified version of sixth-order essentially non-oscillatory (ENO) scheme was used. Direct numerical simulation was performed for turbulence interacting with shock waves with $M_1 = 1.5, 2.0$ and 3.0, where turbulence is fully resolved and the shock wave is captured.

Turbulence kinetic energy is amplified across the shock wave, and the amount of turbulence amplification is consistent with linear analysis. The streamwise velocity fluctuations undergo rapid evolution just behind the shock wave, which can be interpreted as the energy transfer from pressure fluctuations to velocity fluctuations via pressure transport in the shock-normal direction.

The energy spectrum amplification pattern is found to be different for different spectra, and the length scale change across the shock depends on the length scale definition. Most length scales decrease across the shock wave, which confirms the results of LIA and those of shock-resolving simulations with $M_1 \leqslant 1.20$. However, the dissipation length scale and a transverse integral length scale are found to increase slightly in a certain range of shock strengths.

Thermodynamic fluctuations downstream of the shock wave are found to be non-polytropic for strong shock waves, while isentropic fluctuations are found for weak shock waves with $M_1 \leqslant 1.20$. Linear analysis predicts that thermodynamic fluctuations behind the shock contain significant entropy fluctuations leading to non-polytropic behaviour for strong shock waves. The entropy fluctuations are more significant than the acoustic fluctuations beyond $M_1 = 1.65$.

Strikingly, linear theory is found to successfully reproduce most features observed in the interaction of isotropic vortical turbulence with a shock wave, including downstream turbulence evolution and turbulence modification across the shock wave.

The authors would like to acknowledge the financial support from the Air Force Office of Scientific Research under Contract No. F49620-92-J-1028 with Dr Leonidas Sakell as the technical monitor. Thanks are due to Dr Krishnan Mahesh for helpful discussions and comments on a draft of this manuscript. The use of the computer facilities of NAS and NASA-Ames Research Center is also greatly appreciated. A shortened version of this paper was presented at the 32nd Aerospace Sciences Meeting & Exhibit, 1994, Reno, Nevada, USA.

REFERENCES

Andreopoulos, J. & Muck, K.-C. 1987 Some new aspects of the shock-wave boundary layer interaction in compression ramp corner. *J. Fluid Mech.* **180**, 405–428.

Anyiwo, J. C. & Bushnell, D. M. 1982 Turbulence amplification in shock-wave boundary-layer interaction. *AIAA J.* **20**, 893–899.

Barre, S., Alem, D. & Bonnet, J. P. 1996 Experimental study of a normal shock/homogeneous turbulence interaction. *AIAA J.* **34**, 968–974.

Chang, C.-T. 1957 Interaction of a plane shock wave and oblique plane disturbances with special reference to entropy waves. *J. Aero. Sci.* **24**, 675–682.

Debieve, J. F. & Lacharme, J. P. 1986 A shock-wave/free turbulence interaction. *Turbulent Shear Layer/Shock Wave Interactions* (ed. J. Délery). Springer.

Dolling, D. S. & Or, C. T. 1985 Unsteadiness of the shock wave structure in attached and separated compression ramp flows. *Exps. Fluids* **3**, 24–32.

Favre, A. 1965 Équations des gaz turbulents compressibles I. *J. Méc.* **4**, 361–390.

Giles, M. B. 1990 Nonreflecting boundary conditions for Euler equation calculations. *AIAA J.* **28**, 2050–2058.

Hannappel, R. & Friedrich, R. 1994 DNS of a M=2 shock interacting with isotropic turbulence. In *Direct and Large-Eddy Simulation I* (ed. P. R. Voke, L. Kleiser & J.-P. Chollet). Kluwer.

Harten, A. & Osher, S. 1987 Uniformly high-order accurate nonoscillatory schemes, I. *SIAM J. Numer. Anal.* **24**, 279–309.

Hinze, J. O. 1975 *Turbulence*, p. 247. McGraw-Hill.

Honkan, A. & Andreopoulos, J. 1992 Rapid compression of grid-generated turbulence by a moving shock wave. *Phys. Fluids* A **4**, 2562–2572.

Jacquin, L., Blin, E. & Geffroy, P. 1991 Experiments on free turbulence/shock wave interaction. *Eighth Symposium on Turbulent Shear Flows, Munich*, pp. 1-2-1–1-2-6.

Jacquin, L., Cambon, C. & Blin, E. 1993 Turbulence amplification by a shock wave and rapid distortion theory. *Phys. Fluids* A **5**, 2539–2550.

Keller, J. & Merzkirch, W. 1990 Interaction of a normal shock wave with a compressible turbulent flow. *Exps. Fluids* **8**, 241–248.

Kerrebrock, J. L. 1956 The interaction of flow discontinuities with small disturbances in a compressible fluid. PhD Thesis, California Institute of Technology.

Kovásznay, L. S. G. 1953 Turbulence in supersonic flow. *J. Aero. Sci.* **20**, 657–682.

Lee, S. 1992 Large eddy simulation of shock turbulence interaction. *Annual Research Brief*, p. 73–84. Center for Turbulence Research, Stanford University.

Lee, S., Lele, S. K. & Moin, P. 1991*a* Direct numerical simulation and analysis of shock turbulence interaction. *AIAA Paper* 91-0523.

Lee, S., Lele, S. K. & Moin, P. 1991*b* Eddy shocklets in decaying compressible turbulence. *Phys. Fluids* A **3**, 657–664.

Lee, S., Lele, S. K. & Moin, P. 1992*a* Simulation of spatially evolving compressible turbulence and the applicability of Taylor's hypothesis. *Phys. Fluids* A **4**, 1521–1530.

Lee, S., Lele, S. K. & Moin, P. 1993 Direct numerical simulation of isotropic turbulence interacting with a weak shock wave. *J. Fluid Mech.* **251**, 533–562 and corrigendum **264**, 373–374.

Lee, S., Moin, P. & Lele, S. K. 1992*b* Interaction of isotropic turbulence with a shock wave. *Rep.* TF-52. Department of Mechanical Engineering, Stanford University.

Lele, S. K. 1992 Compact finite difference schemes with spectral-like resolution. *J. Comput. Phys.* **103**, 16–42.

Mahesh, K., Lee, S., Lele, S. K. & Moin, P. 1995 The interaction of an isotropic field of acoustic waves with a shock wave. *J. Fluid Mech.* **300**, 383–407.

McKenzie, J. F. & Westphal, K. O. 1968 Interaction of linear waves with oblique shock waves. *Phys. Fluids* **11**, 2350–2362.

Meadows, K. R., Caughey, D. A. & Casper, J. 1993 Computing unsteady shock waves for aeroacoustic applications. *AIAA Paper* 93-4329.

Moore, F. K. 1953 Unsteady oblique interaction of a shock wave with a plane disturbances. *NACA TN*-2879.

Ribner, H. S. 1953 Convection of a pattern of vorticity through a shock wave. *NACA TN*-2864.

Ribner, H. S. 1954 Shock-turbulence interaction and the generation of noise. *NACA TN*-3255.

Ribner, H. S. 1987 Spectra of noise and amplified turbulence emanating from shock-turbulence interaction. *AIAA J.*, **25**, 436–442.

Roberts, T.W. 1990 The behavior of flux difference splitting schemes near slowly moving shock waves. *J. Comput. Phys.* **90**, 141–160.

Rogerson, A. & Meiburg, E. 1990 A numerical study of the convergence properties of ENO scheme. *J. Sci. Comput.* **5**, 151–167.

Rotman, D. 1991 Shock wave effects on a turbulent flow. *Phys. Fluids* A **3**, 1792–1806.

Rusak, Z. & Cole, J. 1993 Interaction of sonic boom with atmospheric turbulence. *AIAA Paper* 93-2943.

Sarkar, S., Erlebacher, G., Hussaini, M. Y. & Kreiss, H. O. 1991 The analysis and modeling of dilatational terms in compressible turbulence. *J. Fluid Mech.* **227**, 473–493.

Sherman, F. S. 1955 A low-density wind-tunnel study of shock-wave structure and relaxation phenomena in gases. *NASA TN*-3298.

Shu, C.-W. 1990 Numerical experimentation on the accuracy of ENO and modified ENO schemes. *J. Sci. Comput*. **5**, 127–149.

Shu, C.-W. & Osher, S. 1989 Efficient implementation of essentially non-oscillatory shock-capturing schemes, II. *J. Comput. Phys.* **83**, 32–78.

Smits, A. J. & Muck, K.-C. 1987 Experimental study of three shock wave/turbulent boundary layer interactions. *J. Fluid Mech.* **182**, 294–314.

Thompson, P. A. 1985 *Compressible-Fluid Dynamics*, p. 183. Maple Press.

Wray, A. A. 1986 Very low storage time-advancement schemes. *Internal Rep.* NASA-Ames Research Center.

Zang, T. A., Hussaini, M. Y. & Bushnell, D. M. 1984 Numerical computations of turbulence amplification in shock-wave interactions. *AIAA J.* **22**, 13–21.

Zeman, O. 1993 A new model for super/hypersonic turbulent boundary layers. *AIAA Paper* 93-0897.